CRACK DRIVING FORCE OF SPECIMENS
WITH SHALLOW CRACK
IN THE UNDERMATCHED WELDED JOINT

ZDRAVKO PRAUNSEIS, VLADIMIR GLIHA

This paper deals with numerical finite element calculations of the crack driving force CTOD–δ_5 for strength-mismatch welded joints. The crack driving force, i.e. the parameter CTOD–δ_5, for bending specimens with shallow cracks in mismatch welded joints is determined at the point of instability when the first ductile or brittle fracture appeared using a numerical model with plane strain conditions at the crack tip. Yield strengths of different microstructures around the crack tip and its actual mechanical properties are taken into account in the finite element model of the specimen. It was shown that by calculated crack driving force, it is possible to predict brittle or ductile fracture initiation of bending specimens with shallow cracks in the weld metal of strength-mismatch welded joints.

HNACIA SILA TRHLINY SKÚŠOBNÝCH TELIES
S PLYTKOU TRHLINOU VO ZVAROVOM SPOJI
S NÍZKOU MEDZOU KLZU ZVAROVÉHO KOVU

Článok sa zaoberá výpočtom hnacej sily trhliny CTOD-δ_5 metódou konečných prvkov vo zvarových spojoch s rozdielnou medzou klzu. Hnacia sila trhliny, t.j. parameter CTOD--δ_5, telesa namáhaného ohybom s plytkou trhlinou vo zvarovom spoji s rozdielnou medzou klzu, sa môže určiť v bode nestability v okamihu vzniku tvárneho alebo krehkého lomu použitím numerického modelu pre podmienky rovinnej deformácie vo vrchole trhliny. Rozdielna medza klzu mikroštruktúr v okolí vrcholu trhliny a ich skutočné mechanické vlastnosti sú zohľadnené v modeli konečných prvkov pre skúšobné teleso. Ukázalo sa, že na základe vypočítanej hodnoty hnacej sily možno predpovedať iniciáciu krehkého alebo tvárneho lomu na telesách namáhaných ohybom s krátkou trhlinou vo zvarovom spoji s rozdielnou medzou klzu.

Dr. Eng. Z. Praunseis, DrSc., University of Osaka, Department of Manufacturing Science, Yamada-oka 2-1, 565-0871 Osaka, Japan.

Doc. Dr. Eng. V. Gliha, DrSc., University of Maribor, Faculty of Mechanical Engineering, Smetanova 17, 2000 Maribor, Slovenia.

List of symbols

a_{exp} — measured crack length

a_{exp}/W — relative depth of crack

$(a/W)_{\text{FEM}}$ — relative depth of crack used in the FEM analysis, $a/W = $ constant

b — uncracked ligament of specimen, $b = W - a_{\text{exp}}$

h — thickness of soft root layer

n — strain hardening coefficient

A — strength coefficient

B — thickness of specimen

F — applied force

H — width of weld joint

L — length of specimen (e.i. SENB, $L = 5 \cdot W$)

R_{p} — yield strength

W — width of specimen

δ — crack tip opening displacement (CTOD)

δ_5 — fracture resistance in terms of CTOD (as determined according to GKSS [3]) = CTOD-δ_5

$\delta_{5\text{FEM}}$ — numerical value of the crack driving force (e.i. CTOD-δ_5)

$\delta_{5\text{i}}$ — value of CTOD-δ_5 at initiation of stable crack growth

$\delta_{5\text{c}}$ — value of CTOD-δ_5 at unstable crack growth and stable crack growth of length less than 0.2 mm

$\delta_{5(\text{i/c})}$ — value $\delta_{5\text{i}}$ or $\delta_{5\text{c}}$

$\delta_{5\text{u}}$ — value of CTOD-δ_5 at stable crack growth of length more than 0.2 mm

$\delta_{0.2}$ — value of CTOD-δ_5 at 0.2 mm of stable crack growth offset to the blunting line

ε — true strain

ε_{f} — fracture strain

ε_{m} — tensile strain

σ_{eq} — effective von Mises stress

Δa — average crack growth including blunting

CTOD — crack-tip opening displacement

FEM — finite element method

GKSS — research institute at Geestacht – Hamburg, Germany

SENB — single edge notch bend

1. Introduction

Safe use of welded structures is dependent on fracture mechanics properties of welded joint. These properties change significantly in the ductile-to-brittle temperature transition region. Fracture (brittle or ductile) should initiate at the instability point, where the driving force acts as a tangent to the CTOD-δ_5 resistance curve [1]. For fracture to occur at the instability point, the driving force – $\delta_{5\mathrm{FEM}}$ must be equal to the material resistance parameter, i.e. the experimentally evaluated fracture toughness – $\delta_{5(\mathrm{i/c})}$.

The purpose of this research was to evaluate the crack driving force – $\delta_{5\mathrm{FEM}}$ numerically for one type of SENB specimens $B \times B$ with a soft root layer (heterogeneous weld) and without it (homogeneous weld) [1, 2], as well as to evaluate the shape and size of yielding zones in the weld metal at the moment of instability when first ductile ($\delta_{5\mathrm{i}}$) or brittle fracture ($\delta_{5\mathrm{c}}$) appeared.

If the numerical driving force values are comparable with the experimental values of fracture toughness – $\delta_{5(\mathrm{i/c})}$, then, on the basis of the calculated crack driving force, a prediction of the brittle or ductile fracture initiation of bending specimens with shallow cracks in the weld metal of strength-mismatch welded joints can be made.
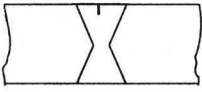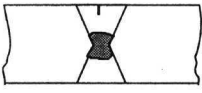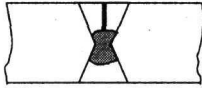
Furthermore, it should be possible to use these results for different models to determine the safe load threshold for real welded structures in the ductile-to-brittle temperature transition region.

2. Numerical modelling of a welded joint

A numerical analysis was performed under plane strain state of SENB specimens ($B \times B$, $B = 36$ mm) with shallow cracks in homogeneous and heterogeneous welds [2]. The application for a plain strain state at the crack tip is recommended by Engineering Treatment Model [3] and standard ASTM E 399-90 [4]. For the analysis, the welds (Table 1) were simplified regarding the geometry and material, e.g. the fusion line between the weld metal and heat affected zone (HAZ) was considered as a straight line. Due to symmetry of SENB specimen (Fig. 1) only one half of the specimen was modelled. Characteristic points for the measurement δ_5 were marked on the specimen surface for CTOD testing [2, 5, 6, 14].

For the numerical modelling of the SENB specimen with a shallow crack in homogeneous and heterogeneous welds, the two-dimensional finite element mesh, as shown in Fig. 1, was used. The nodes of the elements along the axis x (line of the specimen symmetry) and the node in the support position (y axis) were fixed. Furthermore, the specimen was loaded in a three point bending mode with a load applied at mid-span. In the elastic-plastic analyses, the manner in which the load is applied can be very important. If the load is applied to a single node, a local strain concentration can occur, and the elements connected to this node should

Table 1. Results of experimental CTOD-δ_5 fracture toughness and numerical driving force – δ_{5FEM} values for specimens $B \times B$ with shallow crack in homogeneous and heterogeneous welds

Specimen $B \times B$	δ_{5i} [mm]	$\delta_{0.2}$ [mm]	δ_{5c} [mm]	δ_{5u} [mm]	a_{exp}/W	δ_{5FEM} [mm]	$(a/W)_{FEM}$
	0.117	0.191		0.336	0.227	0.106	0.25
	0.100	0.175		0.325	0.239		
	0.103	0.162		0.256	0.261		
	0.089	0.108		0.169	0.255		
	0.089	0.140		0.148	0.417	0.079	0.43
	0.071		0.111		0.446		
	0.062		0.097		0.476		
			0.076		0.450		
			0.042		0.464	0.036	0.48
	0.037		0.044		0.451		
			0.034		0.401		
			0.032		0.423		

yield almost immediately. A better way to apply this boundary condition is to distribute the load over several nodes and specify the elements on which the load remains to act, i.e. $F/2 = F/6 + F/3$ [1], as shown in Fig. 1. For the CTOD-δ_5 evaluation, the mesh was generated with the crack-tip node distanced by 2.5 mm vertically from the specimen symmetry line.

The finite fatigue crack-tip sharpness was simulated by the circle, $r = 0.02$ mm (Fig. 2) and scaled with the initial sharpness of the fatigue crack tip [7], prepared in standard SENB specimen [8, 9]. Previous experimental and FEM analysis [1, 10] showed that the fatigue crack-tip sharpness up to $r = 0.1$ mm did not influence the plastic zone size in the moment of initial fracture. Isoparametric eight-noded finite elements [11] were used for the mesh.

The FEM analysis was used to estimate the influence of the soft root layer with lower yield strength ($R_p \sim 600$ MPa) and soft root layer thickness ($h = 7$ mm) on the crack driving force value CTOD-δ_5 or more specifically, the size and shape of strain hardening zone at crack tip in the moment of fracture initiation (brittle or ductile). For numerical modelling, one specimen with a shallow crack in homogeneous weld and two specimens with a shallow crack in heterogeneous weld were used (Table 1). The actual mechanical properties of the weld filler metal and the soft root weld metal and the base material (HSLA steel with grade HT 80) are summarized in reference [2]. Uniaxial stress-strain behaviour (σ–ε diagram) of the weld filler metal, the soft root weld metal, and the base material for FEM modelling were modelled by linear Hooke law up to the yield point, and in the

strain hardening region by the Ludwik potential equation ($\sigma = A\varepsilon^n$) (Table 2). The values for n (strain hardening coefficient), A (strength coefficient), σ_m (tensile strength), ε_m (tensile strain), σ_f (fracture stress), and ε_f (fracture strain) were calculated by using the experimental σ–ε curves for the weld filler, soft root weld metal, and base material.

For the FEM analysis, the software system ANSYS 5.0 was used [12]. Simulation of SENB specimen loading was done by the gradual increase of force increments F and the calculation of appropriate δ_5 values at each load increment. The system of equations was solved by the Newton-Raphson method, and the von Mises yield criterion was employed. For strains, strain energy, and residual forces, the tolerance criterion was set to 0.1%.

3. Experimental and numerical results

Numerical values of the driving force CTOD-δ_5 for specimens $B \times B$ with shallow crack in homogeneous and heterogeneous welds, together with experimental values CTOD-δ_5 are given in Table 1. The relationship betw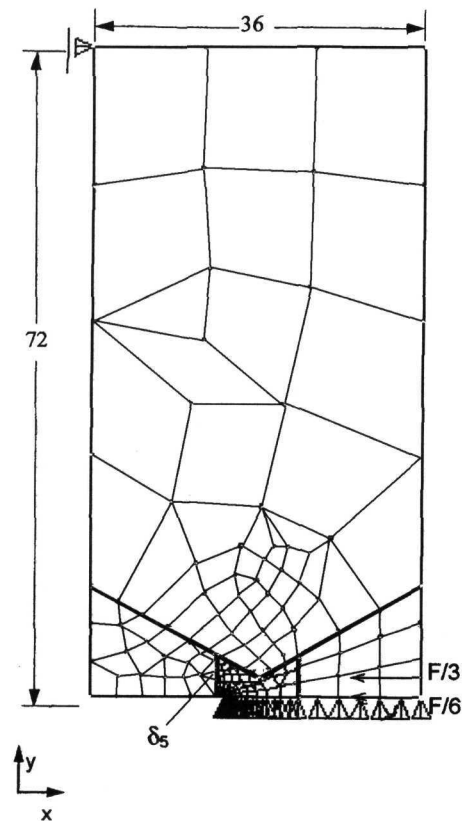een the strain value at the crack tip and the fracture strain ε_f has been chosen as the criterion for material decohesion in simulations of the SENB specimen loading. It was assumed that the fracture is initiated (either brittle or ductile) at the moment when the strain value at the crack tip reaches the fracture strain ε_f. Applying this criterion, the critical strain level should be $\varepsilon \geq \varepsilon_f$ at the region just ahead of the crack tip since the fracture strain ε_f can be reached in a single point. The size of the critically stressed region has to be much smaller than the plastic zone size. In Fig. 2, A denotes the critical region ahead of the crack tip. The size of the region is approximately 0.04×0.02 mm, which is about 2% of the plastic zone size when the load reaches the critical

Fig. 1. Finite element mesh for bend specimen $B \times B$ with a shallow heterogeneous welds.

STRESS CONTOURS
PLASTIC STRAINS
VIEW : 5.00E-15
RANGE : 7.05E+00

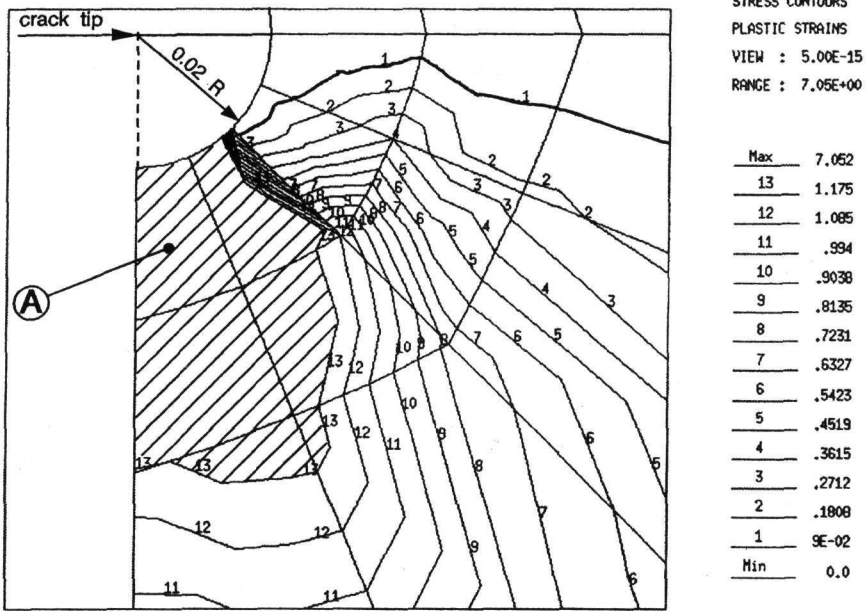|	
Max	7.052
13	1.175
12	1.085
11	.994
10	.9038
9	.8135
8	.7231
7	.6327
6	.5423
5	.4519
4	.3615
3	.2712
2	.1808
1	9E-02
Min	0.0

Fig. 2. Strains at crack tip in the moment of fracture ($\delta_{5\text{FEM}} = 0.036$ mm) for specimen with heterogeneous weld and relative crack depth $(a/W)_{\text{FEM}} = 0.48$. In the region A strains are $\varepsilon > \varepsilon_f$.

Table 2. Mechanical properties calculated by using experimental σ–ε curves of weld filler metal and soft root weld metal, and base material

Value	Base material	Weld filler metal	Soft root layer
n	0.09068	0.10109	0.04980
A [MPa]	1183.5	1143.8	876
σ_m [MPa]	909	871	757
ε_m	0.05332	0.06555	0.0572
σ_f [MPa]	1497	1530	1330
ε_f	1.010	0.95	1.175

specimen fracture value. This is about five times smaller than the crack-length increment $\Delta a = 0.2$ mm, which is the value at the stable crack-growth initiation [9].

A comparison between numerical and experimental curves F-CTOD is shown in Figs. 3–5. The moment, when the critical strain ahead of the crack tip is reached
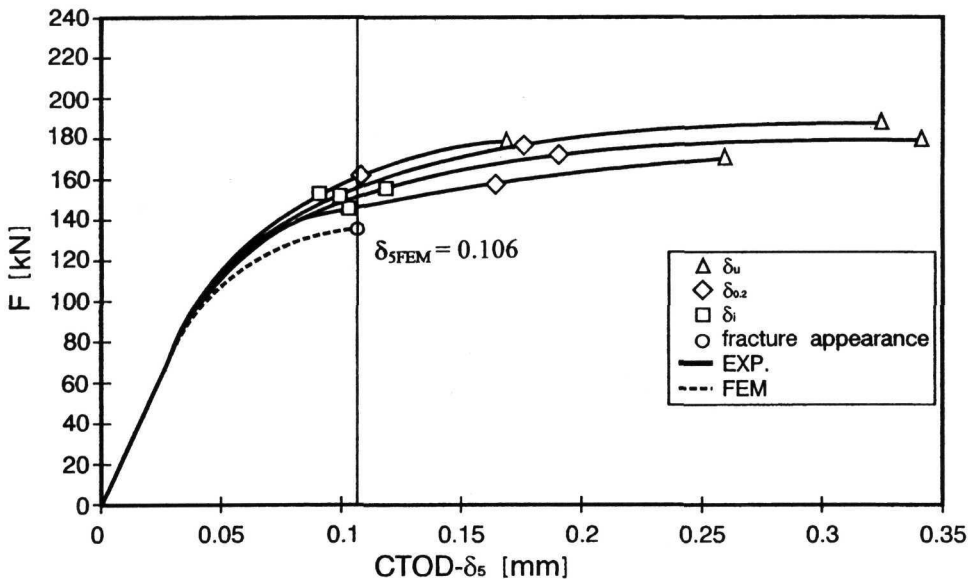
Fig. 3. Comparison of experimental fracture toughness δ_{5i} and numerical driving force – δ_{5FEM} values for specimen with shallow crack $(a/W)_{FEM} = 0.25$ in homogeneous weld.

$(\varepsilon \geq \varepsilon_f)$ during simulated SENB specimen loading, is denoted by circle (o) on the simulation curves F-CTOD and represents a numerical value of the crack driving force δ_{5FEM}. Comparison of δ_{5FEM} with the experimental values of CTOD-δ_5 was possible only up to the point of fracture initiation, δ_{5i} or δ_{5c}, on experimental curve F-CTOD. The geometry of the real SENB specimens changed abruptly (in the case of brittle fracture appearance) or continuously changed (slow crack growth) after fracture initiation. From the comparison of the results for the crack driving force δ_{5FEM} and experimental fracture toughness $\delta_{5(i/c)}$, given in Table 1, it is clear that the crack driving force δ_{5FEM} for SENB specimens with homogeneous and heterogeneous welds, as well as for different crack depths a_{exp}/W, was larger than most experimental fracture toughness values $\delta_{5(i/c)}$. Analysis of the experimental results [1, 2] showed that the CTOD values depend on constraint [13] at the crack tip due to different crack depth a_{exp}/W, coefficient of weld shape $H/(W - a_{exp})$ and local plastic constraint factor in the weld root due to strength mismatching. The constraint at the crack tip also had a significant influence on the numerical values of crack driving force δ_{5FEM}, being higher for the SENB specimens with shallow cracks (Table 1), observed by comparing the numerical curves F-CTOD
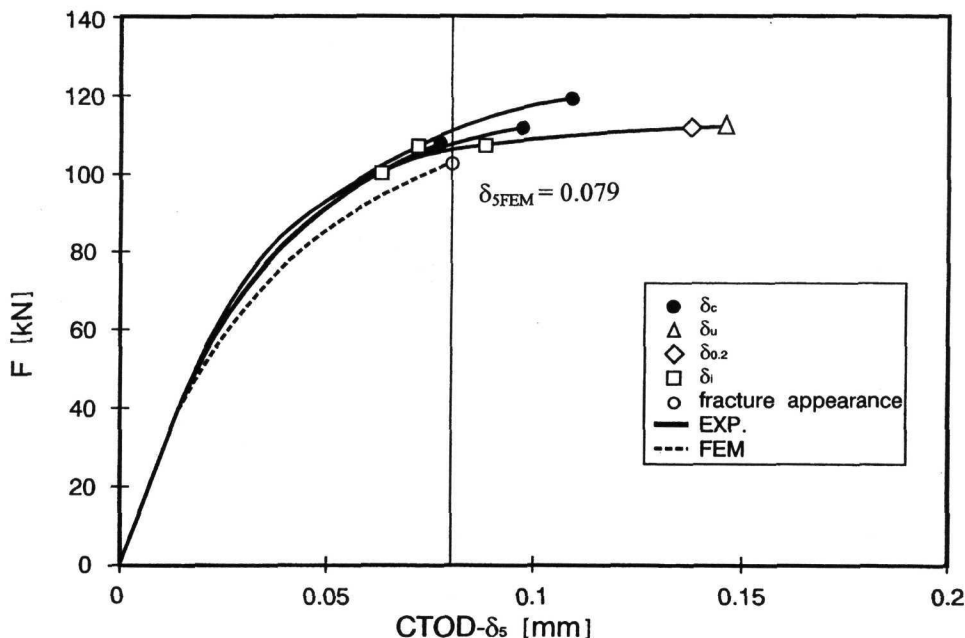
Fig. 4. Comparison of experimental fracture toughness $\delta_{5(i/c)}$ and numerical driving force – δ_{5FEM} values for specimen with shallow crack $(a/W)_{FEM} = 0.43$ in heterogeneous weld.

(Figs. 3–5). Therefore, only the comparison of crack driving forces δ_{5FEM} for the specimens with the same crack depth in heterogeneous welds was reasonable.

Discrepancies between the numerical and experimental curves F-CTOD, as well as between the experimental results of fracture toughness $\delta_{5(i/c)}$ and the numerical values of crack driving force δ_{5FEM}, are due to the following reasons. The role of hardening exponent n in homogeneous and heterogeneous welds is not quite clear. The round tensile specimens were not taken exactly from the regions where the fatigue crack tip was positioned and represent only the average mechanical properties of weld metal regions [1]. In this example the hardening exponent n was overestimated, producing higher numerical values for the crack driving force δ_{5FEM} since the fracture strain values ε_f were overrated. On the contrary, conservative values of hardening exponent n resulted in the underestimated fracture strain ε_f, producing lower values for the crack driving force δ_{5FEM}. The real mechanical properties of homogeneous and heterogeneous welds, used for numerical simulation of SENB specimen loading, were obtained at room temperature while the real CTOD values were obtained at $-10\,^\circ$C. The temperature difference also caused
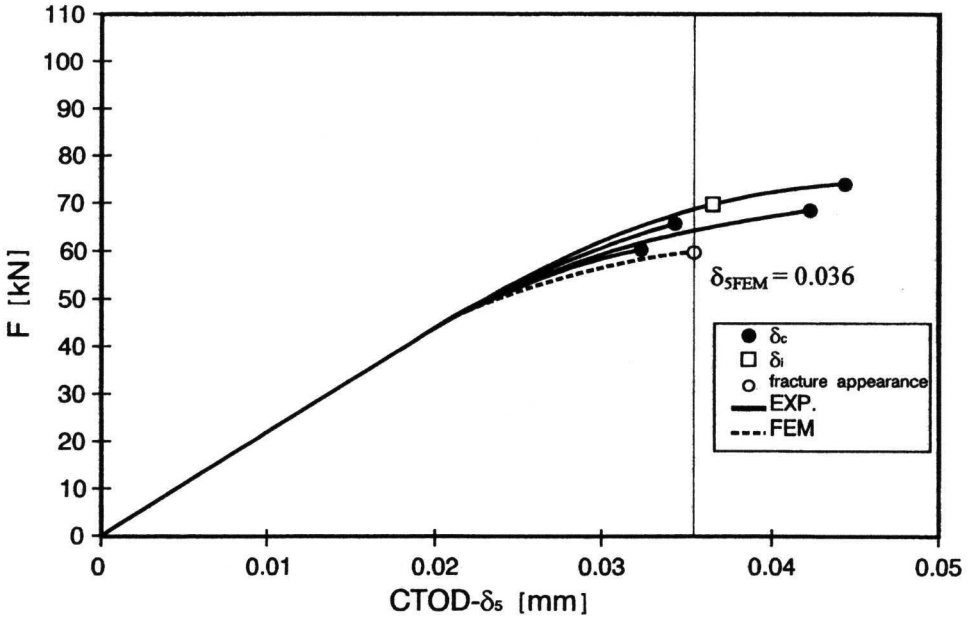
Fig. 5. Comparison of experimental fracture toughness $\delta_{5(i/c)}$ and numerical driving force – δ_{5FEM} values for specimen with shallow crack $(a/W)_{FEM} = 0.48$ at soft root layer boundary.

the overestimation of n. It is well known that the yield and tensile strengths [13] increase with a decrease of the temperature, whereas ductility (i.e. fracture strain ε_f) decreases. From Figs. 3–5, large differences are noticeable between experimental values of $\delta_{5(i/c)}$ and numerical values of crack driving force δ_{5FEM} for SENB specimens with a crack positioned in heterogeneous weld metal than for those with a crack positioned in homogeneous weld metal.

A fracture toughness $\delta_{5(i/c)}$ larger than the crack driving force δ_{5FEM} was noticed in the set of specimens with a heterogeneous weld and a crack depth of $a_{exp}/W \sim 0.43$ in the specimen having $\delta_{5i} = 0.089$ mm and $a_{exp}/W = 0.417$, where the largest fatigue crack tip distance from the soft root layer boundary was observed (Table 1, Fig. 4). For this specimen the crack depth a_{exp}/W was also smaller than the crack depth $(a/W)_{FEM}$, which was exactly 0.43. This is another reason for obtaining a value of the fracture toughness δ_{5i} larger than the crack driving force δ_{5FEM}. The microstructure effect on $\delta_{5(i/c)}$ was less pronounced in this set of specimens because all fatigue crack tips were positioned in the bainitic microstructure of weld filler metal [1].
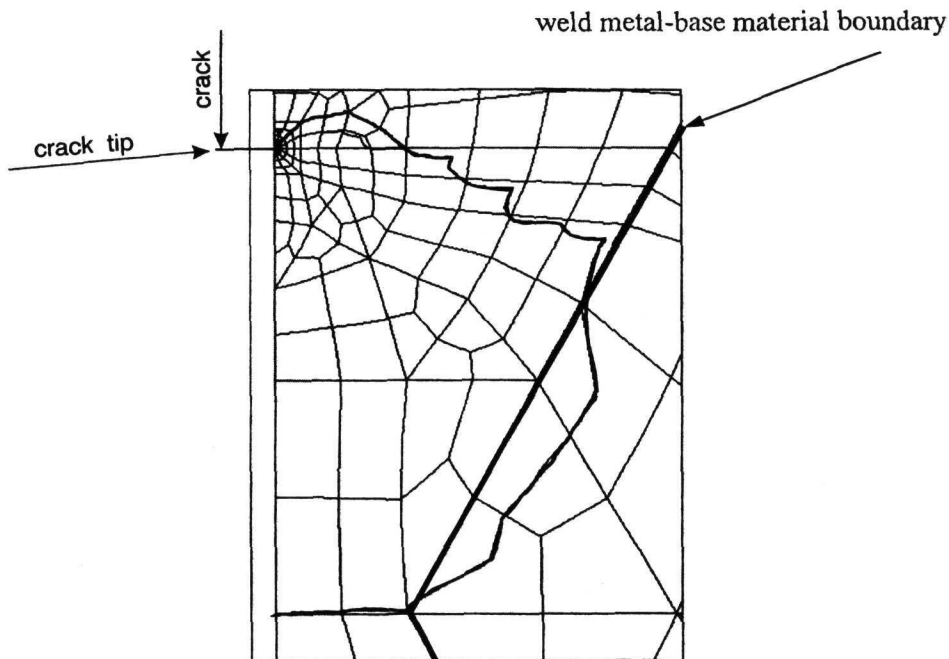
Fig. 6. Crack-tip plastic zone size and shape in the moment of fracture ($\delta_{5\mathrm{FEM}} = 0.106$ mm) for specimen $B \times B$ with homogeneous weld and relative crack depth $(a/W)_{\mathrm{FEM}} = = 0.25$.

The effect of microstructure on CTOD values was more pronounced in a set of specimens with crack depth $a_{\mathrm{exp}}/W \sim 0.48$ and fatigue crack tip position at the soft root layer boundary (Table 1, Fig. 5) since the microstructure at crack tip changed considerably with a small increase of crack depth a_{exp}/W. The variable soft root layer thickness, which was a consequence of soft root layer build-up (welding sequence of passes [1]), prevented the fatigue crack tip positioning exactly at the soft root layer boundary in either specimen. In the two specimens with $\delta_{5\mathrm{i}}$ $= 0.037$ mm and $\delta_{5\mathrm{c}} = 0.042$ mm (Table 1), the fatigue crack tip was positioned just above the soft root layer in a higher toughness, bainitic microstructure weld filler metal boundary (Fig. 6 – Detail A and B in reference [2]). The difference in crack-depth value $(a_{\mathrm{exp}}/W < (a/W)_{\mathrm{FEM}})$ caused the fracture toughness $\delta_{5(\mathrm{i}/\mathrm{c})}$ to be higher than the crack driving force $\delta_{5\mathrm{FEM}}$. Since FEM analysis was performed using a crack depth of 0.48 $(a/W)_{\mathrm{FEM}}$ and the crack tip positioned soft root layer with a ferritic microstructure (Fig. 7 – Detail A and B in reference [2]), the value of $\delta_{5\mathrm{FEM}}$ is smaller. A reasonable and more realistic comparison between the crack
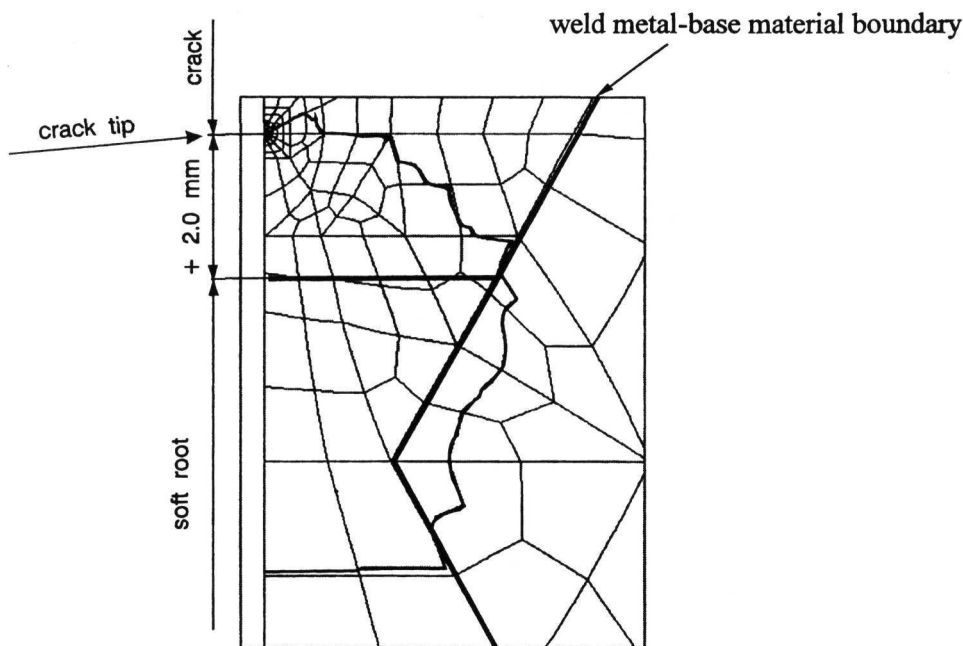
Fig. 7. Crack-tip plastic zone size and shape in the moment of fracture ($\delta_{5\text{FEM}} = 0.079$ mm) for specimen $B \times B$ with heterogeneous weld and relative crack depth $(a/W)_{\text{FEM}} = 0.43$.

driving forces $\delta_{5\text{FEM}}$ and the fracture toughness $\delta_{5(\text{i/c})}$ values was made for those specimens with the same crack depths $(a_{\text{exp}}/W = (a/W)_{\text{FEM}})$ and the crack tip positioned in the same microstructure. For the specimens with $\delta_{5c} = 0.032$ mm and $\delta_{5c} = 0.034$ mm (Table 1), it was shown by fractographical and metallographical analysis [1] that the fatigue crack was located in the soft root layer (Fig. 7 in reference [2]), reducing fracture toughness δ_{5c} values and thus making the comparison with crack driving force $\delta_{5\text{FEM}}$ more realistic.

For the SENB specimens with shallow crack $(a_{\text{exp}}/W \sim 0.25)$ in a homogeneous weld metal, it was important to position the fatigue crack tip in the bainitic microstructure (Fig. 4 in reference [2]) and that the values of δ_{5u} were determined at the stable crack-growth initiation (Table 1, Fig. 3). The initiation values δ_{5i} were smaller than the crack driving force $\delta_{5\text{FEM}}$ for three specimens, but higher for the specimen with $\delta_{5i} = 0.117$ mm. Higher fracture toughness δ_{5i} of this specimen was caused by the lowest crack depth a_{exp}/W (Table 1) of all specimens. Therefore, the constraint effect on CTOD values was also the lowest [1, 2].
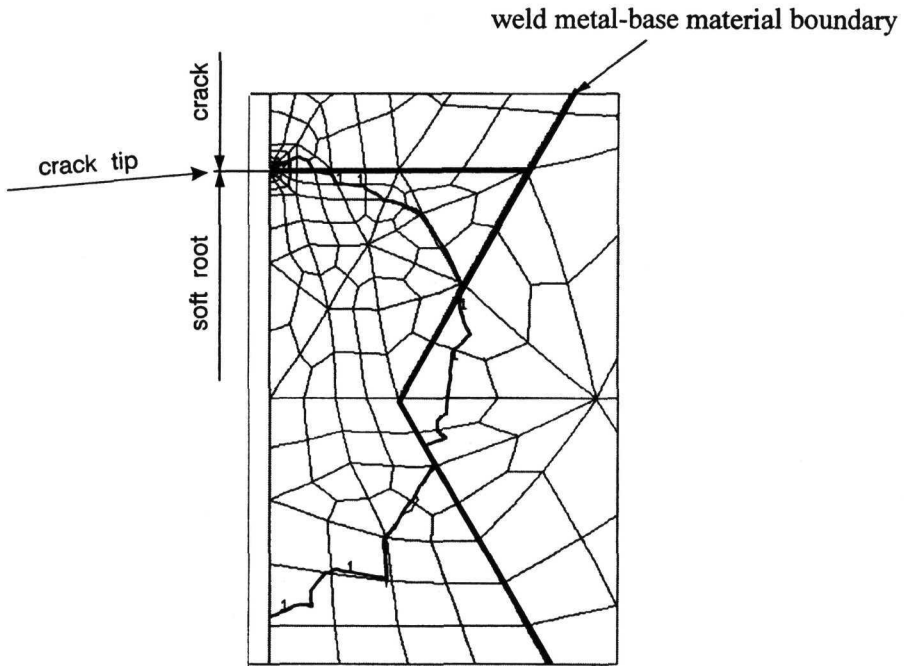
Fig. 8. Crack-tip plastic zone size and shape in the moment of fracture ($\delta_{5FEM} = 0.036$ mm) for specimen with heterogeneous weld and relative crack depth $(a/W)_{FEM} = 0.48$.

The model of the material behaviour, obtained on basis of weld tensile loading (σ–ε diagram) and used to simulate SENB specimen loading, was not precise enough for simulating the real material behaviour at the crack tip with respect to the position of neutral axis of the SENB specimen bending. The neutral axis separates tensile and compressive stresses in the middle of the ligament b of the SENB specimen and simultaneously shifts with crack propagation. Tensile stresses exist in the region between the crack tip and the neutral axis while compressive stresses are present in the remaining half of the ligament, i.e. between the loading point and the neutral axis. Therefore in loading the SENB specimen, approximately 50% of applied force was spent on tensile stresses while the other 50% was spent for compressive stresses. Compressive stresses limit the spreading of the plastic strain zone at the crack tip, requiring a higher force during specimen bending to obtain the same plastic zone size compared to the simulation using the "pure" tensile model of material behaviour. Since the specimen was laid on rollers which pressed into the surface, a higher bending force was required for the experiment
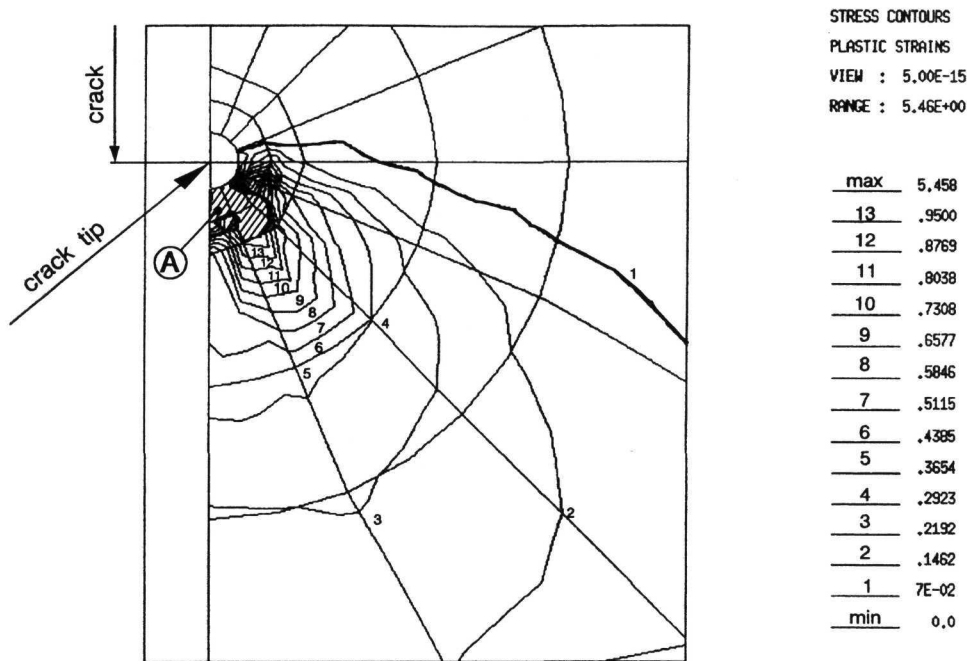
Fig. 9. Strains at the crack tip in the moment of fracture ($\delta_{5FEM} = 0.106$ mm) for specimen $B \times B$ with homogeneous weld and relative crack depth $(a/W)_{FEM} = 0.25$. In the region A strains are $\varepsilon > \varepsilon_f$.

than in the simulation which neglected sample positions.

Figures 6–8 show the size and the shape of plastic regions at the crack tip in the moment of ductile or brittle fracture initiation of specimens with crack tip position in homogeneous and heterogeneous weld metal. The size and the shape of plastic zone was evaluated using the contour of the yield strength ($\sigma_{eq} = R_p$). The yield strength for homogeneous and heterogeneous welds are given in reference [2] and the hardening exponents n are given in Table 2. From these figures, it is clear that the material flow in the initiation moment was not limited to the homogeneous and heterogeneous weld metal, but it also spread across the fusion line into the base material causing an increase in the plastic zone size. For the FEM calculation, the homogeneous and heterogeneous welds were simplified in regard to the geometry and material [1], e.g. higher strength of the HAZ. The higher HAZ strength presented a barrier to further plastic flow, and hardening was not taken into account. A lower degree of plastic flow was achieved in specimens with a homogeneous weld than in specimens with a heterogeneous weld. This was due

to a higher degree of hardening (higher n) for the homogeneous weld, which can be observed from a comparison of plastic zone sizes and plastically deformed base material zones (Figs. 2 and 9). Also, the higher average "loading capacity" in the homogeneous weld was a factor in the smaller plastic flow. The homogeneous weld was made by the same consumable (WELTEC B 575) and had a higher average hardening capability compared to heterogeneous weld, which was "weakened" by a soft root layer (WELTEC B 370) [1], evident in the comparison of the hardening exponents n (Table 2).

4. Conclusions

1. The relatively good approximation of the experimental results by the numerical simulation of crack driving force CTOD-δ_5 indicates the possibility of using FEM for evaluating the crack initiation driving force for mismatch welded joints.

2. A heterogeneous undermatched welded joint with soft root layer is not appropriate for X-groove shape because the yielding and hardening are mostly limited to the narrowest root region of weld joint. The high strain field occurs in the root weld metal, causing higher constraint of the low-strength microstructure in the weld root. Hence, yielding and hardening of low-strength root region are retarded while in the high strength regions yielding already started at the same stress level.

3. On the basis of above-mentioned analysis it can be concluded that the results of crack driving force of strength-mismatch welded joints are strongly affected by:
   – the microstructure at the crack tip,
   – the constraint due to different crack depth a_{exp}/W,
   – the weld metal width $H/(W - a_{exp})$.

Further activity will be dedicated to determining the influence of the different undermatch levels in soft root layer on the fracture behaviour of a V-groove shape welded joint towards crack propagation through microstructures of the heat-affected zone.

REFERENCES

[1] PRAUNSEIS, Z.: The influence of strength undermatched weld metal containing heterogeneous regions on fracture properties of HSLA steel weld joint. [Dissertation in English]. University of Maribor, Slovenia 1998.

[2] PRAUNSEIS, Z.: Kovove Mater., *37*, 1999, p. 266.

[3] SCHWALBE, K.-H.: The Engineering Treatment Model (ETM) Method for Assessing the Significance of Crack-Like Defects in Engineering Structures. Version ETM 95/1 and ETM 95/2. Geesthacht, Research Center of Materials 1996.

[4] ASTM E 399-90: Standard Test Method for Plane-Strain Fracture Toughness of Metallic Materials. Annual Book of ASTM Standards. Philadelphia, Pergamon Press 1990.

[5] GKSS: Displacement Gauge System for Applications in Fracture Mechanics. Patent Publication. Geesthacht, Research Center of Materials 1991.

[6] PRAUNSEIS, Z.—GUBELJAK, N.: In: Proceedings of the 37. International Conference on Experimental Stress Analysis. Ed.: Plánička, F. VŠB-TU Ostrava 1999, p. 167.

[7] MUKAI, Y.—NISHIMURA, A.: Transactions of the Japan Welding Society, *14*, 1983, p. 353.

[8] BS 7448: Fracture Mechanics Toughness Test. Part 2. Method for Determination of K_{IC}, Critical CTOD and Critical J Values of Welds in Metallic Materials. Cambridge, TWI Abingdon Hall 1997.

[9] ASTM E 1290-93: Standard Test Method for Crack-Tip Opening Displacement (CTOD) Fracture Toughness Measurement. Philadelphia, ASTM 1993.

[10] DAWES, M. G.: Metal Construction and British Weld Journal, *9*, 1990, p. 319.

[11] OWEN, D. R. J.—HINTON, E.: Finite Elements in Plasticity: Theory and Practice. Department of Civil Engineering, University College of Swansea, U.K. 1990.

[12] ANYS/ED 5.0.: Manual Guide. London, Taylor & Francis Ltd. 1995.

[13] ANDERSON, T. L.: Fracture Mechanics Fundamentals and Applications. 2nd Edition. Los Angeles, Kluwer Academic Publishers 1994.

[14] GUBELJAK, N.: International Journal of Fracture, *100*, 1999, p. 155.